Contents lists available at ScienceDirect

Arabian Journal of Chemistry

journal homepage: www.ksu.edu.sa

Original article

Synthesis, characterization and adsorption of Pb(II), Cd(II) and Cu(II) by red mud/polyacrylic acid/sodium carboxymethyl cellulose hydrogel

Dong Zhao [a,b,c], Hua Deng [a,b,c,*], Wei Wang [a,b,c], Lening Hu [a,b,c], Shunyun Ye [a,b,c], Jiahui Fu [a,b,c], Shuyun Zhang [a,b,c]

[a] Guangxi Key Laboratory of Environmental Processes and Remediation in Ecologically Fragile Regions, Guangxi Normal University, Guilin 541004, China
[b] Key Laboratory of Ecology of Rare and Endangered Species and Environmental Protection, Guangxi Normal University, Guilin 541004, China
[c] College of Environment and Resources, Guangxi Normal University, Guilin 541004, China

ARTICLE INFO

Keywords:
Red mud
Hydrogel
Heavy metal ions
Adsorption performance
Adsorption mechanism

ABSTRACT

Heavy metal pollution in water and pollution hazards caused by red mud disposal are urgent environmental problems to be solved. Red mud waste can be utilized as resources by preparing hydrogels. By employing free radical polymerization, a red mud/polyacrylate/sodium carboxymethyl cellulose hydrogel (RMAAC) was synthesized using red mud (RM) as the main component, sodium carboxymethyl cellulose (SCMC) as the grafting substrate, N, N'-methylene bisacrylamide (MBA) as the crosslinking agent, and potassium persulfate (KPS) as the initiator. The proportions of MBA, KPS, and SCMC were optimized using the response surface method. The adsorption kinetics and isothermal adsorption model were applied to analyze the adsorption characteristics, while XRD, FTIR, SEM-EDS, and XPS characterization methods were employed to study the adsorption mechanism. The results demonstrated that the optimal proportions of MBA, KPS, and SCMC in RMAAC were determined to be 0.15 %, 0.2 %, and 1.5 %, respectively, and the addition of 0.5 % RM to enhance the adsorption performance of the hydrogel. The adsorption processes of Pb(II), Cd(II), and Cu(II) by RMAAC followed the pseudo-second-order kinetic model and the Langmuir model, suggesting chemisorption through a single molecular layer as the main adsorption mechanism. The maximum theoretical adsorption capacities of the three heavy metal ions at 25°C were determined to be 730.16, 292.71, and 215.37 mg/g, respectively. It was found that RMAAC exhibited a higher affinity toward Pb(II) compared to Cu(II) and Cd(II). Characterization analyses revealed that ion exchange and coordination chelation were the predominant mechanisms involved in the adsorption of Pb(II), Cd(II), and Cu(II) by RMAAC.

1. Introduction

The discharge of hazardous substances into water bodies from increased anthropogenic activities has caused a growing concern of heavy metal pollution (Singh et al., 2023). Heavy metal ions possess high toxicity and are non-degradable, posing a significant threat to both ecosystems and human health (Malik et al., 2019). For instance, Common heavy metal ions include Pb and Cd, which have biological half-lives of 7–16 years and 150 years respectively within the human body (Abdel-Magied et al., 2022), while excessive Cu metal can lead to gastrointestinal discomfort, liver and kidney damage, as well as impairment of the mental system (Noor et al., 2024; Vardhan et al., 2019). The urgency in addressing the detrimental effects of heavy metal pollution has led to the development of various technologies for removing heavy metal ions from water bodies, including adsorption, ion exchange, membrane separation, electrochemical treatment, and chemical precipitation (Bashir et al., 2019; Fu et al., 2022). Among these methods, adsorption demonstrates advantages in terms of operational ease, availability, cost-effectiveness, and efficiency (Rajendran et al., 2022; Zhang et al., 2021). Therefore, the removal of heavy metal ions through adsorption represents an effective and straightforward technology (Jiang et al., 2024).

In recent years, there has been significant attention directed towards low-cost adsorbents (Bilal et al., 2021), including both biological and natural materials. Among natural materials, red mud, zeolite, clay, cellulose, and chitosan are commonly utilized as adsorbents (Chakraborty et al., 2022). Red mud is an alkaline solid waste generated during alumina production through the Bayer process (Arroyo et al.,

* Corresponding author.
E-mail address: denghua@mailbox.gxnu.edu.cn (H. Deng).

https://doi.org/10.1016/j.arabjc.2024.106067
Received 28 June 2024; Accepted 16 November 2024
Available online 19 November 2024

2020). The discharge of red mud has been steadily increasing, necessitating the development of targeted approaches for its comprehensive resource utilization to mitigate pollution hazards associated with its disposal (Niu and Lin, 2024; Wang et al., 2021). Red mud is widely utilized in industries such as building materials and ceramics due to its abundant content of active mineral components (Wang et al., 2019). It possesses a porous structure, rich metal and non-metallic oxides, and a substantial specific surface area (Pan et al., 2023). Furthermore, red mud can also be employed as an environmental remediation material, thereby contributing to environmental governance and ecological restoration. Heavy metal ions can exchange with mineral ions in red mud or precipitate with alkaline ions in red mud (Qi et al., 2024). For instance, Liu et al. synthesized a red mud/polyacrylic acid (RM/PAA) composite material through in-situ grafting polymerization in a reversed-phase suspension system (Liu et al., 2020). This composite material exhibited efficient adsorption capacity for Cd (II) ions in aqueous solutions, reaching a maximum adsorption capacity of 96.15 mg/g. Tsamo et al. investigated the use of raw and hydrochloric acid-modified red mud (RMA) as an adsorbent for removing Cr (VI), Cu (II), and Pb (II) from aqueous solutions, and the adsorption process was consistent with a pseudo-second-order kinetic model (Tsamo et al., 2018). Another study by Ahmed et al. a synthesized red mud/biochar (RM/BC) composite material using straw as raw material (Ahmed et al., 2023). Compared with the original BC (287.67 mg/g), the composite material exhibited a higher adsorption capacity for Pb (II) at 426.84 mg/g and contained a greater amount of oxygen-containing functional groups.

The direct use of primary red mud for pollutant removal in water can be challenging due to its fine particle morphology, which can lead to filtration difficulties and secondary pollution (Agrawal and Dhawan, 2021; Liu and Naidu, 2014). Therefore, the development of innovative hybrid composite materials using red mud holds great significance for its comprehensive utilization. The combination of industrial waste and natural polymer organic matter in the preparation of adsorbents allows for the effective utilization of waste resources. Researchers have also explored the development and use of red mud in hydrogel form (Sandu et al., 2017). This approach not only improves the adsorption and mechanical properties of the hydrogels, but also addresses the problem of difficult solid–liquid separation in industrial solid waste applications (Lunardi et al., 2024). For example, Arnaldo et al. prepared a homogeneous hybrid polyacrylamide hydrogel (PAAm) by using red mud and ferrosilicon-manganese powder (FeSiMn), which resulted in a swelling index nearly 1.5 times larger than that of conventional hydrogels (Ramírez et al., 2022).

Hydrogels, intricate three-dimensional networks formed by physically or chemically cross-linking polymer chains, are extensively utilized in treating heavy metal ions in wastewater due to their porous structure, polar functional groups, and adaptability to the environment (Tang et al., 2020a). The fundamental components required for hydrogel preparation include monomers, crosslinking agents, and initiators (Darban et al., 2022). Hydrogel preparation methods can be categorized into physical crosslinking and chemical crosslinking, with free radical polymerization being widely popular due to the diverse range of monomers, synthesis techniques, and simple preparation (El Sayed, 2023). The selection of polymeric materials containing specific groups is a simple and eco-friendly approach for hydrogel preparation (Li et al., 2023). Sodium carboxymethyl cellulose (SCMC), known for its flexible geometry, cost-effectiveness, and natural cellulose, has emerged as a promising adsorbent matrix (Li et al., 2020). Incorporating acrylic acid (AA) as a functional monomer modification introduces hydrophilic groups and enhances hydrophilicity (Zhang et al., 2019). The use of potassium persulfate (KPS) as an initiator in hydrogel preparation offers the benefits of non-toxicity and high chemical resistance, ensuring the safety and stability of the hydrogels in various applications (Sun et al., 2022).

In this study, red mud (RM) and sodium carboxymethyl cellulose (SCMC) were used as substrate materials for grafting. Acrylic acid (AA) served as the functional monomer, N,N'-methylenebisacrylamide (MBA) as the cross-linking agent, and potassium persulfate (KPS) as the initiator. By means of a free radical polymerization reaction, red mud-polyacrylic acid-sodium carboxymethyl cellulose hydrogels (RMAAC) were prepared for the purpose of removing Pb(II), Cd(II), and Cu(II) from aqueous solutions. Response surface methodology was employed to optimize the optimal combination ratio of each component in RMAAC. The study systematically investigated the effects of pH, time, and temperature on the adsorption performance. In addition, X-ray diffraction (XRD), Fourier transform infrared spectroscopy (FTIR), Scanning electron microscope-Energy dispersive spectrometer (SEM-EDS), and X-ray photoelectron spectroscopy (XPS) characterization techniques were employed to analyze the adsorption characteristics of these three heavy metals using RMAAC materials.

Table 1
Box-Behnken design factors and levels.

Number	Factor	Unit	Factor level		
			−1	0	1
A	Proportion of MBA	%	0.10	0.15	0.20
B	Proportion of KPS	%	0.15	0.20	0.25
C	Proportion of SCMC	%	0.50	1.50	2.50

2. Materials and methods

2.1. Materials

Bayer red mud (RM) was sourced from Guangxi Huayin Aluminum Co., LTD. Acrylic acid (AA) and potassium persulfate ($K_2S_2O_8$) were purchased from Xilong Chemical Co., LTD. N,N'-methylene bisacrylamide ($C_7H_{10}N_2O_2$) was obtained from Shanghai Maclin Biochemical Technology Co., LTD., and sodium carboxymethyl cellulose (SCMC) was purchased from Sinopsin Chemical Reagent Co., LTD. All the aforementioned reagents were of analytical purity. Various concentrations of heavy metal ions were prepared using deionized water (DI) in combination with nitrogen oxides of the corresponding heavy metals.

2.2. Preparation of RMAAC

2.2.1. Preparation of experimental materials

The RMAAC was synthesized via free radical polymerization. The raw red mud was obtained by natural drying and grinding of Bayer process red mud, followed by sieving through an 80 mesh (0.178 mm) standard screen. SCMC and RM were dissolved in water and stirred until uniformly mixed. Next, 0.833 g of NaOH was accurately weighed and fully dissolved in 2 mL of water. Then, 2 mL of AA was slowly added dropwise into the NaOH solution, and the mixture was allowed to stand for 1 h after complete dissolution. The evenly mixed SCMC and RM solution was then added to the above mixture, followed by the sequential addition of MBA and KPS. The resulting hydrogel after polymerization was subjected to ultrasonic treatment at 60°C for 2 h. Finally, the residual material on the surface of the hydrogel was cleaned with ethanol solution multiple times and dried in an oven at 70°C until a constant weight was achieved.

2.2.2. Optimum preparation experiment of RMAAC

A three-factor, three-level experimental design was employed to determine the optimal usage amount of each component in RMAAC through response surface analysis based on the Box-Behnken central composite design. The selected variable factors and corresponding levels are summarized in Table 1. The independent variables included the cross-linking agent MBA, the initiator KPS, and SCMC, represented as factors A, B, and C, respectively. The adsorption capacities of these three heavy metals were considered as the dependent variables, denoted as

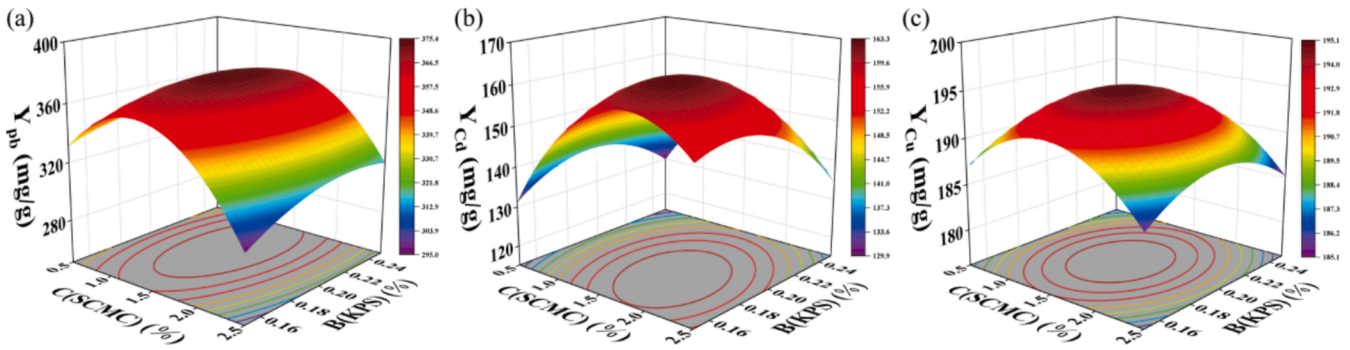

Fig. 1. The 3D schematic diagram illustrating the response surface of RMAAC adsorption for three heavy metals using C (SCMC) as the x-axes and B (KPS) as the y-axes: (a) Y_{Pb}, (b) Y_{Cd}, (c) Y_{Cu}.

Y_{Pb}, Y_{Cd}, and Y_{Cu}. Subsequently, 0.5 %, 1 %, and 2 % RM were added under the optimized conditions mentioned earlier. Finally, RMAAC exhibiting the best performance was determined through heavy metal ion adsorption performance tests. The test procedures and data regarding the physical properties of RMAAC can be found in the supplementary material (Text S1).

2.3. Batch adsorption and multi-heavy metal system experiment

Solutions containing Pb(II), Cd(II), and Cu(II) were prepared at concentrations of 600, 200, and 200 mg/L, respectively. The pH levels were adjusted within the range of 2 to 6 to investigate the influence of different pH conditions on both adsorption capacity and removal efficiency. Furthermore, the adsorption characteristics of RMAAC were further investigated by preparing solutions containing Pb(II) with different concentrations (ranging from 20 to 1200 mg/L), as well as Cd

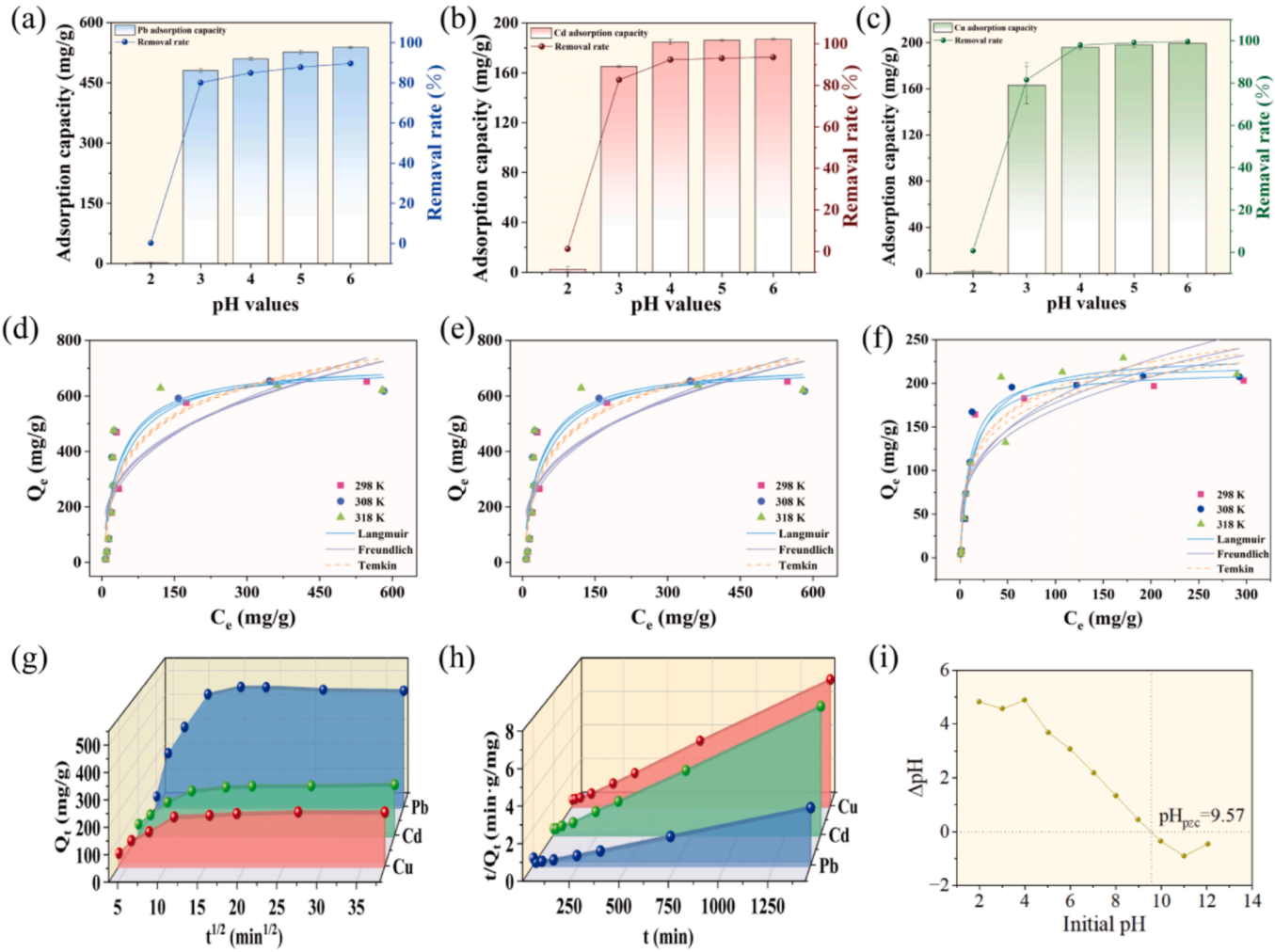

Fig. 2. RMAAC adsorption characteristics of three heavy metals: (a) Effect of different pH on adsorbed Pb(II), (b) Effect of different pH on adsorbed Cd(II), (c) Effect of different pH on adsorbed Cu(II), (d) Adsorption isotherm of Pb(II) adsorption, (e) Adsorption isotherm of Cd(II) adsorption, (f) Adsorption isotherm of Cu(II) adsorption, (g) Intra-particle diffusion model fitting, (h) Pseudo-second-order kinetic model fitting, (i) Point of zero charge (pH_{pzc}).

(II) and Cu(II) (ranging from 5 to 500 mg/L). These adsorbents were thoroughly mixed at different temperatures (ranging from 25 to 45 °C) for a period of 24 h. Afterward, samples were taken from each solution and analyzed. The obtained data were subsequently analyzed using Langmuir, Freundlich, and Temkin model equations separately to characterize the adsorption isotherm behavior. Additionally, solutions of Pb(II), Cd(II), and Cu(II) were prepared with concentrations of 500, 200, and 200 mg/L, respectively. Samples were taken at different time points (ranging from 15 to 1440 min) for determination. The collected data were analyzed by fitting it to pseudo-first-order kinetics, pseudo-second-order kinetics, and intra-particle diffusion model, respectively, to gain a deeper insight into the adsorption process. The equations utilized in the batch adsorption experiments, as well as the method for determining the point of zero charge (pH_{pzc}) of RMAAC, can be located in the supplementary material (Text S2).

To study the selective adsorption of RMAAC for heavy metals, solutions containing these three heavy metals with a concentration of 200 mg/L were prepared. The removal rates of these three heavy metals were measured in both single-component and multi-component systems. Throughout all the aforementioned experiments, the dosage of RMAAC was maintained at a 1 g/L solid–liquid ratio and the experiments were conducted under controlled conditions of 25 °C and 150 r/min agitation.

2.4. Characterization and analysis

The experimental data underwent statistical analysis and processing utilizing Microsoft Excel 2020, SPSS 26.0, and Origin 17.0 software. Additionally, Design-Expert 8.0.6 software was employed for response surface program design and the creation of 3D schematic drawings. XRD, FTIR, SEM-EDS, and XPS characterization techniques were used to investigate the adsorption characteristics. Specific models and manufacturers of the characterization methods used can be found in the reference material (Text S3).

3. Results and discussion

3.1. RMAAC optimization preparation

According to the Box-Behnken central composite design scheme, Design-Expert 8.0.6 composite was used to formulate the response surface methodology. The obtained results are presented in Table S1. The regression equation derived from fitting the experimental data of the response surface methodology is as follows:

$Y_{Pb} = 373.90 + 3.31A + 5.37B\text{-}13.34C + 8.59AB + 3.48AC + 4.70BC + 34.16A^2\text{-}11.17B^2\text{-}44.18C^2$.

$Y_{Cd} = 195.08 + 0.27A\text{-}0.28B\text{-}0.53C + 1.33AB\text{-}1.07AC + 0.13BC + 0.27A^2\text{-}3.58B2\text{-}5.68C^2$.

$Y_{Cu} = 161.86 + 3.05A\text{-}4.60B + 6.17C + 0.40AB + 2.65AC\text{-}4.00BC + 2.07A^2\text{-}8.68B^2\text{-}16.48C^2$.

Variance analysis was conducted on the Y_{Pb} (Table S2), Y_{Cd} (Table S3) and Y_{Cu} (Table S4) models for adsorption of these three heavy metals. The obtained P values for these models were 0.0055, 0.001, and 0.0169 (P values < 0.05) consecutively. The P values for the missing items were 0.3153, 0.1441, and 0.2855 (P values > 0.05), indicating a well-fitting effect of the model. The analysis revealed that the factors C (SCMC), B(KPS), and A(MBA) have a significant impact on the adsorption of these three heavy metals, with the order of significance being C (SCMC) > B(KPS) > A(MBA). The three-dimensional response surface diagram, as depicted in Fig. 1, allows for a visual evaluation of the interaction between the usage of each monomer. The results of the response surface analysis indicated that the optimal values for each variable were MBA 0.15 %, KPS 0.2 %, and SCMC 1.5 %. Under this optimal solution, as shown in Table S1, the prepared RMAAC exhibited adsorption capacities of 381.7, 169.8, and 195.8 mg/g for Pb(II), Cd(II), and Cu(II), respectively.

On the basis of the above methodology, RMAAC was prepared by incorporating different concentrations (0.5 %, 1 %, and 2 %) of RM. The removal efficiencies of these three heavy metals were recorded and are presented in Table S5. When compared to the absence of RM addition, the removal rates for Pb(II) increased from 93.23 % to 95.47 %, for Cd (II) from 90.43 % to 94.50 %, and for Cu(II) from 87.52 % to 90.56 %. It was noted that the predominant adsorption mechanism was due to the polymer, and the inclusion of 0.5 % RM further enhanced the adsorption performance of the hydrogel. Conversely, the incorporation of 1 % and 2 % RM resulted in reduced adsorption performance, leading to local accumulations. Consequently, the subsequent experiments selected the addition of 0.5 % RM as the optimum concentration.

3.2. Adsorption performance of Pb(II), Cd(II), and Cu(II) by RMAAC

3.2.1. Adsorption effects, adsorption isotherms and adsorption kinetics

As depicted in Fig. 2a–c, the adsorption capacity of RMAAC shows a continuous increase as the pH value rises from 2 to 6. This trend remains consistent across the removal of the three heavy metal ions. When the pH value is 2, RMAAC exhibits the lowest removal rate for the three heavy metals, with the adsorption capacities of Pb(II), Cd(II), and Cu(II) are 1.35, 2.50 and 1.45 mg/g, respectively. When the pH value is 3, there is a significant improvement in the removal rates of the three heavy metal ions by RMAAC, with the adsorption capacities of these three heavy metals are 480.50, 165.35 and 163.35 mg/g, respectively. The removal rates are 80.1 %, 82.7 % and 81.6 %, respectively. As the pH value exceeds 3, the increase in adsorption capacity of RMAAC becomes slower and tends to stabilize. Fig. 2i illustrates the initial pH of RMAAC versus the final pH after 24 h. The difference between the two values, known as ΔpH, is crucial for determining the point of zero charge (pH_{pzc}). This parameter is essential for understanding the surface charge of the material and the type of adsorption that occurs. The pH_{pzc} of RMAAC was determined to be 9.57. It is worth noting that a pH greater than 6 tends to result in the formation of water-insoluble metal oxides and hydroxide precipitates (Akl et al., 2022). In this study, the pH level significantly impacts the adsorption performance of RMAAC, with the amount of heavy metals being adsorbed continuous increasing as the pH value rises. This phenomenon can be explained by the presence of a low pH solution (Ke et al., 2024). The presence of a strong acidic environment can cause the crystal structure to deteriorate and result in the protonation of functional groups, such as amino and carboxylic groups, on the surface of RMAAC. This leads to an increase in positive charges (Elwakeel et al., 2023). Consequently, electrostatic adsorption is reduced or the functionality of these functional groups in interacting with heavy metal ions is weakened. Moreover, at low pH values, H^+ ions compete with heavy metal ions for adsorption sites, thereby diminishing the adsorption capacity. As the pH value gradually rises, the concentration of H^+ ions decreases, prompting the deprotonation of functional groups and consequently enhancing the adsorption capacity (Yin et al., 2023). Within the pH range of 3 to 6, RMAAC maintains a removal rate above 80 % for all three heavy metals, indicating that it possesses sufficient adsorption sites. Therefore, RMAAC exhibits a wide pH application range for these three heavy metals. The adsorption performance of RMAAC does not significantly decrease with decreasing pH values within this range.

The adsorption characteristics of RMAAC were further examined, and the experimental data obtained from adsorption isotherms were analyzed using the Langmuir, Freundlich, and Temkin models for fitting purposes. The results of isotherm fitting (Fig. 2d–f) and fitting data (Table S6) were obtained. Based on the fitting results, the adsorption processes of these three heavy metals by RMAAC at different temperatures exhibited similar trends. At a temperature of 298 K, the Langmuir model provided higher correlation coefficients ($R^2 > 0.9$) for the adsorption of these three heavy metals by RMAAC, and the corresponding values were found to be 0.977, 0.902, and 0.942, respectively. In contrast, the Freundlich model yielded lower fitting correlation coefficients: 0.752, 0.726, and 0.809, while the Temkin model resulted in

Table 2
Comparison of adsorption capacities of various adsorbents for Pb(II), Cd(II), and Cu(II) ions.

Adsorbents	Maximum adsorption capacity (mg/g)			Optimum pH	References
	Pb(II)	Cd(II)	Cu(II)		
Red mud/ polyacrylic acid/ sodium carboxymethyl cellulose hydrogel	730.16	292.71	215.37	6	Present study
Chitosan/acrylic acid/ formaldehyde hydrogel beads	21.38	24.80	-	10	Azeem et al., 2022
Carboxymethyl cellulose/ chitosan catecholyl hydrogel	204.00	167.00	196.00	7	Zou, 2024
Enteromorpha polysaccharides-based hydrogel	166.70	76.90	83.30	4.5	Wen et al., 2023
Polyacrylic acid/ carboxymethyl starch /Fe_3S_4 magnetic hydrogel	233.68	-	42.72	6	Feng et al., 2023
Chitosan/itaconic acid/ methacrylic acid hydrogel	-	285.70	-	5.5	Milosavljevic et al., 2010
Chitosan/ polyacrylamide semi-interpenetrating polymer network hydrogel	61.41	-	72.39	7	Zhao et al., 2021
Vinyl alcohol/2-acrylamido-2-methyl-1-propanesulfonic acid hydrogel	340.00	155.10	-	6	Ma et al., 2018b
Polyvinyl alcohol/ chitosan/ polydopamine-functionalized graphene oxide hydrogel	210.94	236.20	210.94	5.5	Li et al., 2019
Chitosan/calcium alginate/ bentonite composite hydrogel	434.89	102.38	115.30	5	Lin et al., 2021
Chitosan/sodium alginate/calcium ion double-network hydrogel	176.50	81.25	70.83	5	Tang et al., 2020b
Chitin/chitosan-based aerogel	-	-	59.21	5	Kuang et al., 2023
Colloidal silica and sodium hydroxide modified red mud	564.97	-	-	6	Lyu et al., 2021
Magnetic 4A-zeolite based on red mud	116.81	131.96	136.33	-	Xie et al., 2018
MnO_2-modified red mud	721.35	-	-	8	Bai et al., 2023

correlation coefficients of 0.849, 0.883, and 0.910. At temperatures of 308 K and 318 K, the correlation coefficients remained unchanged. The Langmuir model was determined to be more appropriate for describing the adsorption process of these three heavy metals by RMAAC. The theoretical maximum adsorption capacities at 25°C were determined to be 730.16, 292.71, and 215.37 mg/g, respectively. These results indicate monolayer adsorption, where heavy metal ions are uniformly adsorbed on the hydrogel surface (Bai et al., 2022). Additionally, the K_L values of the fitting parameters ranged from 0 to 1, indicating that the adsorption process facilitated the removal of pollutants (Omrani and Nezamzadeh-Ejhieh, 2020).

To better accurately characterize the adsorption process of heavy metals by RMAAC, the adsorption data for these three heavy metals were analyzed using the kinetic models to fit the experimental results. The time-dependent variation of the heavy metal adsorption capacity of RMAAC is depicted in Fig. 2. It is evident that the adsorption behavior of RMAAC towards the three heavy metals is consistent, with the adsorption capacity increasing as the contact time increases. The adsorption process comprises two distinct stages: a rapid adsorption stage and a gradual adsorption stage (Fig. 2g). Within the first 120 min of initial contact, the adsorption of these three heavy metals by RMAAC exhibits a rapid adsorption stage. Subsequently, the adsorption rate enters a slower stage until it approaches adsorption equilibrium at around 240 min. The fitting parameters for the pseudo-first-order kinetic and the pseudo-second-order kinetic were determined, and the results are presented in Table S7. The analysis of the first-order kinetic yielded theoretical maximum adsorption capacities of 477.66, 196.18, and 190.85 mg/g for these three heavy metals, with corresponding correlation coefficients (R^2) of 0.886, 0.938, and 0.959. On the other hand, the pseudo-second-order kinetic model exhibited a high degree of fitting accuracy in describing the adsorption process (Fig. 2h). The theoretical maximum adsorption capacities obtained from fitting the pseudo-second-order kinetic were 522.73, 213.95, and 209.02 mg/g for these three heavy metals, with correlation coefficients of 0.964, 0.990, and 0.998. The results of fitting the pseudo-second-order kinetic were found to be closer to the actual experimental results of the maximum adsorption capacities for these three heavy metals. Therefore, the pseudo-second-order kinetic model emerges as a more precise descriptor of the adsorption process for these three heavy metals by RMAAC, affirming its character as chemical adsorption (Liu, 2023). Furthermore, the pseudo-second-order kinetic model offers a comprehensive depiction of the adsorption reaction's different stages, encompassing liquid film diffusion, surface adsorption, and internal diffusion. The analysis of the intra-particle diffusion model results (Table S7) indicated the presence of two distinct stages as revealed by the fitted data. The initial stage encompasses the migration of heavy metal ions from the liquid film to the surface of RMAAC, while the subsequent stage involves their movement from the surface of RMAAC into the particles (Cortés et al., 2023). The fitting parameters, where $k_{d1} > k_{d2}$ and $C_1 < C_2$, indicate that liquid film diffusion predominantly influences the adsorption process (Xu et al., 2024). These two stages solely represent the intra-particle diffusion process. However, considering the non-origin intercept, it can be inferred that intra-particle diffusion is not the sole mechanism governing the adsorption process (Zhou et al., 2022). Surface adsorption is likely to have a noteworthy impact. Upon contact between heavy metal ions in the solution and RMAAC, there is a rapid adsorption onto the surface of RMAAC, after which diffusion occurs within the three-dimensional structure of the hydrogel. This implies that the process is initially governed by external mass transfer and subsequently transitions to intra-particle diffusion mass transfer.

Table 2 presents the maximum adsorption capacities of various adsorbents, including hydrogels and red mud, for Pb(II), Cd(II), and Cu(II) ions as reported by RMAAC and other studies. When compared to these other adsorbents, RMAAC exhibits superior adsorption capacity.

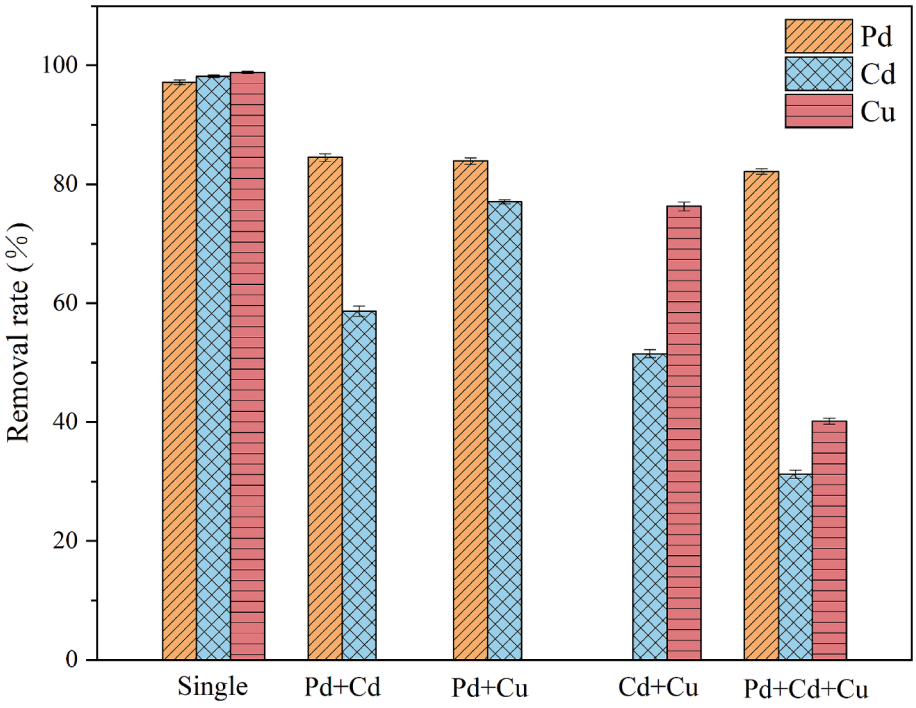

Fig. 3. Removal of heavy metals by RMAAC in a multivariate system. In the monadic system, the three heavy metals (Pd, Cd, and Cu) are separated individually. The heavy metals present in the binary and ternary systems are indicated at the x-axes.

3.2.2. Multi-heavy metal system experiment

There are often multiple heavy metal ions present in actual wastewater, making it practically significant to study the adsorption characteristics of RMAAC in a multi-heavy metal system. As depicted in Fig. 3, it presents the adsorption performance of RMAAC in different heavy metal systems. In a single system, RMAAC exhibits a higher level of adsorption for three heavy metals, indicating that it is more efficient in treating single heavy metal wastewater compared to other multi-component systems. However, in complex environments, the different affinity between different heavy metal ions and the surface functional groups of hydrogels leads to an ion competition effect. By conducting this study, the binding ability of heavy metals and RMAAC in the multi-heavy metal system was determined to be: Pb(II) > Cu(II) > Cd(II). In the binary system and ternary system, the adsorption performance of

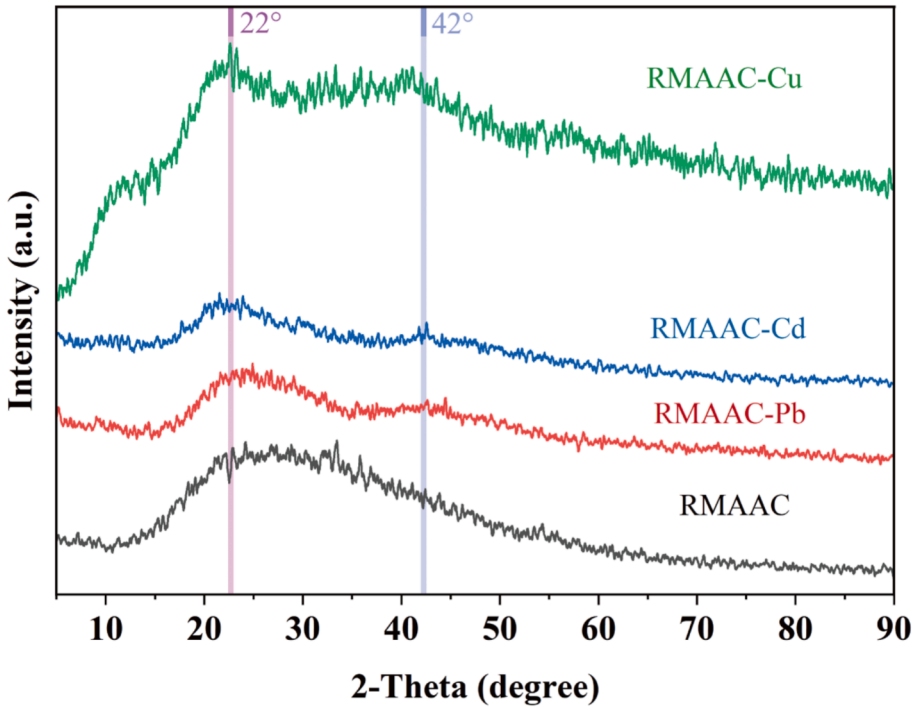

Fig. 4. XRD patterns of RMAAC before and after adsorption of Pb(II), Cd(II) and Cu(II). The bands, from bottom to top, are as follows: RMAAC (black) before adsorption, RMAAC-Pb (red) after the adsorption of Pb, RMAAC-Cd (blue) after the adsorption of Cd, and RMAAC-Cu (green) after the adsorption of Cu.

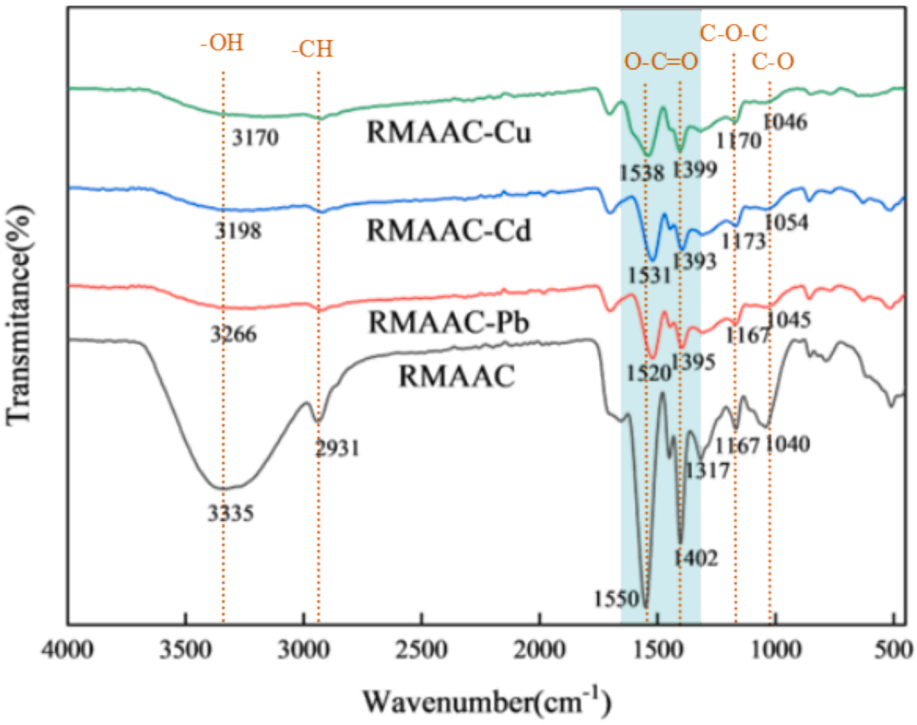

Fig. 5. Infrared spectrum of RMAAC before and after adsorption of Pb(II), Cd(II), and Cu(II).

RMAAC for Cd(II) and Cu(II) is reduced, while the adsorption of Pb(II) remains at a high level. This indicates that Pb(II) has a more competitive advantage in the multicomponent system, and RMAAC can provide more adsorption sites for Pb(II). The adsorption of Pb(II) is minimally impacted by the presence of other metal elements. Within the Cu-Cd system, RMAAC demonstrates better adsorption effectiveness for Cu (II). The hydration radius sizes for the three heavy metal ions follow the order: Pb(II) < Cu(II) < Cd(II) (Nassef et al., 2024). It has been observed that metal ions with smaller hydration radii exhibit stronger affinity towards adsorbents (Ma et al., 2021). Numerous investigations have indicated that electronegativity plays a crucial role in influencing the selective adsorption of metal ions by hydrogels (Liu et al., 2023; Zhang et al., 2022). Specifically, higher electronegativity corresponds to greater affinity. The electronegativity values for the three heavy metal ions are Pb(II) (2.3), Cu(II) (1.9), and Cd(II) (0.7), respectively (Zhang et al., 2024). These values align with the experimental findings regarding the selective adsorption characteristics.

3.3. Characterization and mechanism analysis of RMAAC

3.3.1. XRD characterization

XRD analysis was employed to analyze the crystallinity of RMAAC before and after the adsorption of the three heavy metals. The obtained results are presented in Fig. 4. In the XRD pattern of RMAAC, a broad diffraction peak ranging from 15° to 40° (2-Theta) was observed. This peak can be attributed to the amorphous structure of the polymer formed through the process of polymerization (Liu et al., 2022). Subsequent to the adsorption of Pb(II) and Cd(II) by RMAAC, there was a noticeable decrease in the intensity of the broad diffraction peak (from 25° to 35°) compared to the pre-adsorption state. Additionally, a new peak emerged at 2-Theta values ranging from 35° to 50° (a clear peak signal appears around 2-Theta = 42°). This new signal peak suggests that RMAAC effectively loaded Pb(II) and Cd(II) (Liang et al., 2017). Moreover, upon the adsorption of Cu(II) by RMAAC, a distinct peak signal appeared at 2-Theta = 22°, providing further evidence for the successful adsorption of Cu(II) onto the RMAAC adsorbent.

3.3.2. FTIR characterization

In order to confirm that RMAAC successfully introduced functional groups of AA and SCMC and participated in the adsorption process of heavy metals, infrared spectral analysis was conducted on the hydrogels before and after the adsorption of three heavy metals by RMAAC. The results are presented in Fig. 5. It can be observed from the spectrum diagram of RMAAC that the wide peak near 3335 cm^{-1} is caused by the O–H stretching vibration of the hydroxyl group. The absorption peak at 2931 cm^{-1} corresponds to the tensile vibration of C–H. The absorption peaks at 1550 and 1402 cm^{-1} mainly arise from the symmetric and asymmetric stretching vibrations of O-C = O in carboxylic acid groups. The absorption peak at 1167 cm^{-1} represents the antisymmetric bridge stretching vibration of C-O-C. Additionally, the absorption peak at 1317 cm^{-1} corresponds to the C-O stretching vibration in the carboxylic acid group (Enoch and Somasundaram, 2023; Jiao et al., 2022; Jing et al., 2023; Liang et al., 2023; Xi et al., 2022). Therefore, the carboxylic acid groups of AA and the hydroxyl and carboxylic acid groups of SCMC were successfully introduced into RMAAC hydrogel, indicating that acrylic acid and sodium carboxymethyl cellulose were successfully grafted during the polymerization reaction to prepare RMAAC (Bao et al., 2020; Wu and Li, 2023). After the adsorption of these three heavy metals by RMAAC, the broad peaks near 3335 cm^{-1} moved to 3266, 3198 and 3170 cm^{-1}, respectively, with weakened peak intensities. This suggests that a significant number of hydroxyl groups in RMAAC participated in the adsorption of heavy metals (Hong et al., 2019). The absorption peaks at 1550 and 1402 cm^{-1} shifted to 1520, 1531, 1538 cm^{-1} and 1395, 1393, 1399 cm^{-1}, respectively, with reduced peak strengths. This demonstrates the involvement of a substantial number of carboxylic acid groups in RMAAC in the adsorption of heavy metals (Gururajan and Belur, 2018). Through the analysis of the aforementioned absorption peaks, it can be concluded that both the hydroxyl group (O–H) and the carboxyl group (O-C = O) in RMAAC play a crucial role in the adsorption process.

3.3.3. SEM-EDS characterization

SEM-EDS analysis was performed on the RMAAC both before and after the adsorption of these three heavy metals. The results are

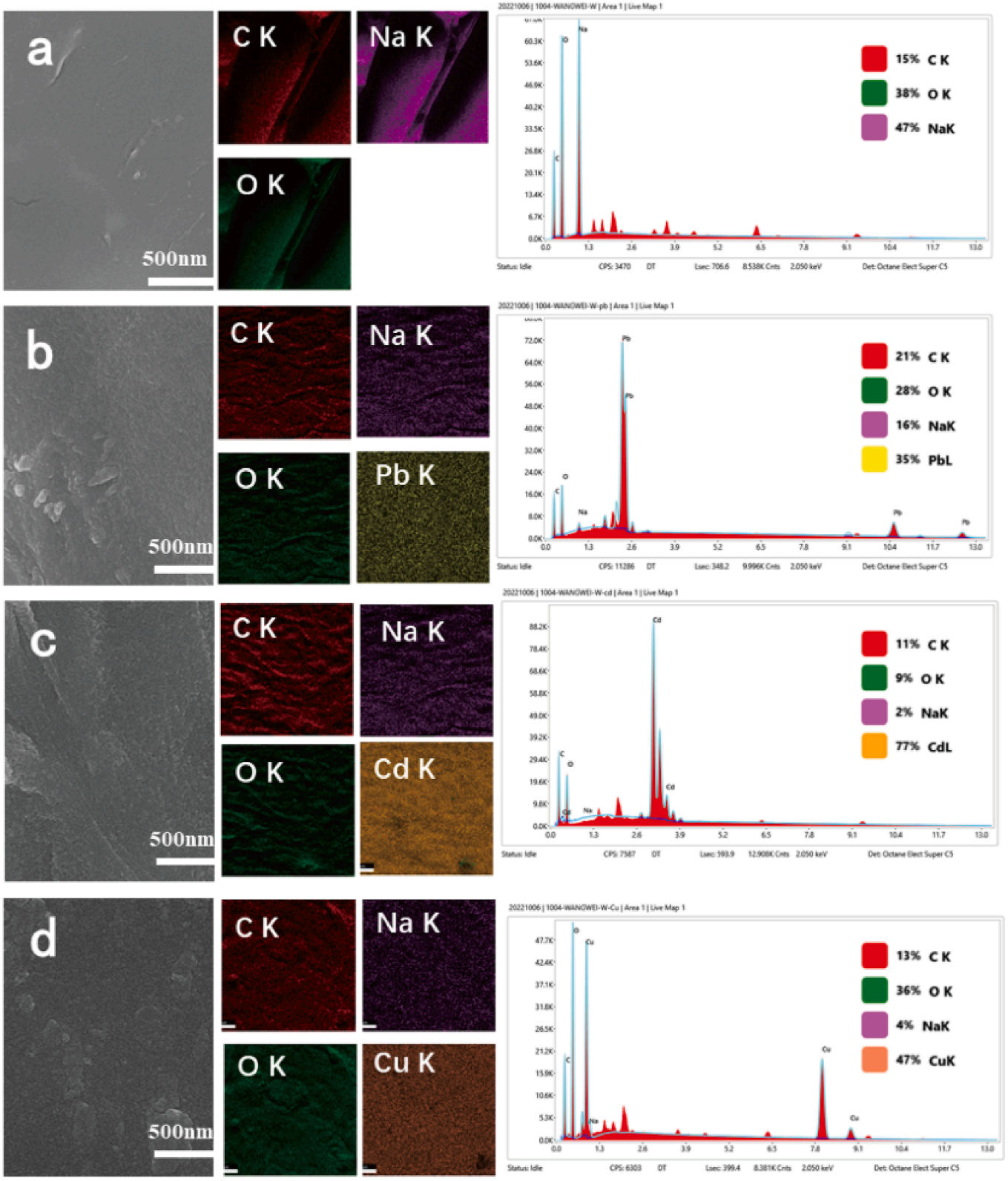

Fig. 6. SEM-EDS images of RMAAC before and after adsorption: (a) Pre-adsorption, (b) After adsorption of Pb(II), (c) After adsorption of Cd(II), (d) After adsorption of Cu(II).

presented in Fig. 6. As can be observed from the figure, the surface of the RMAAC material appears smooth and even, exhibiting a uniform texture without any visible agglomeration phenomenon (Fig. 6a). However, after the adsorption of these three heavy metals by the RMAAC, the surface morphology undergoes significant changes. Specifically, the surface becomes wrinkled and the formation of coarse granules is evident (Fig. 6b–d). These observations strongly suggest that such alterations are induced by the adsorption of heavy metal ions onto the material (Zhao et al., 2023). Upon comparing the variations in content before and after adsorption, it was discovered that the proportion of

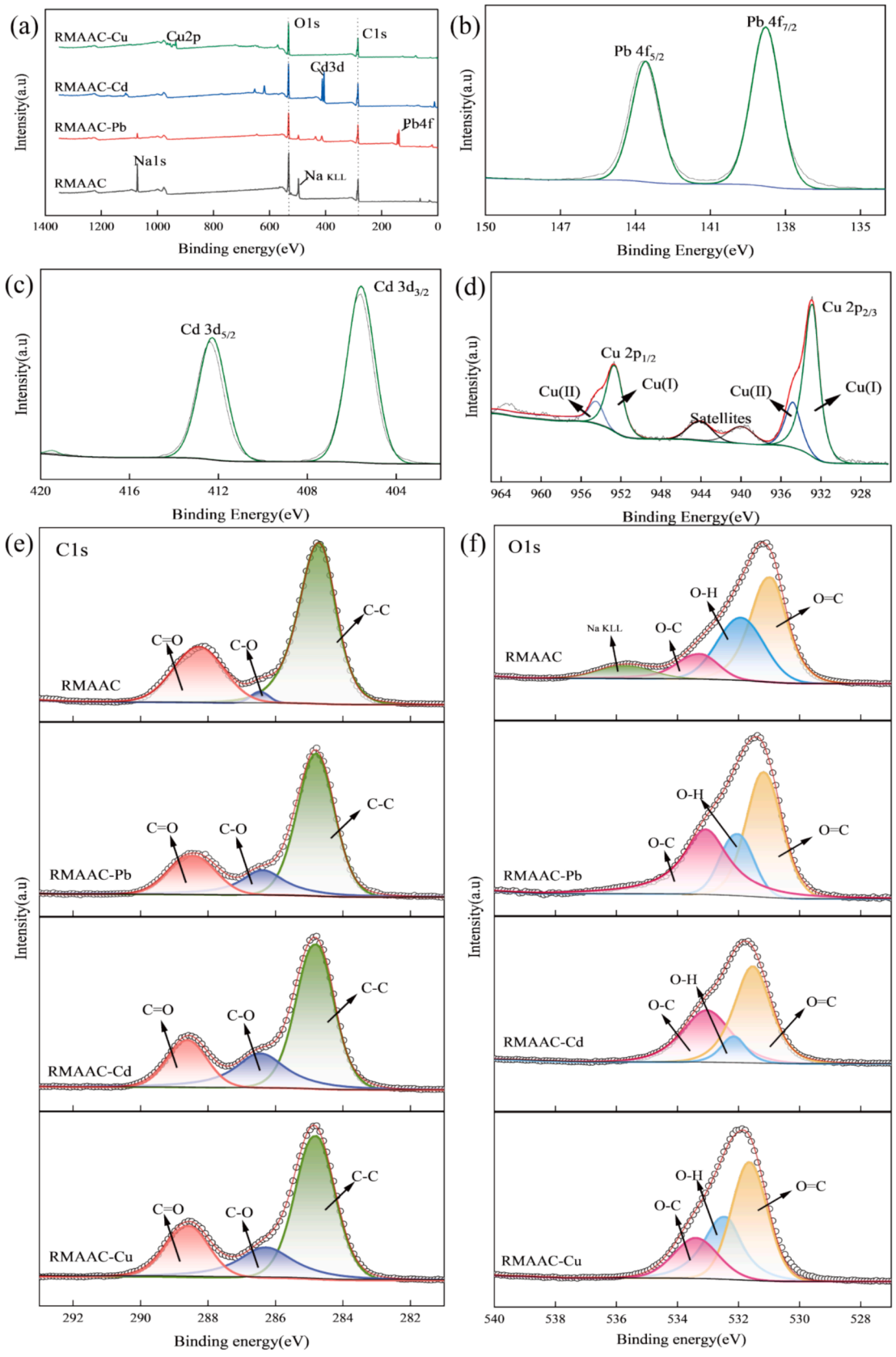

Fig. 7. XPS spectrum of RMAAC before and after adsorption: (a) XPS total spectrum, (b) Pb4f, (c) Cd3d, (d) Cu2p, (e) C1s, (f) O1s.

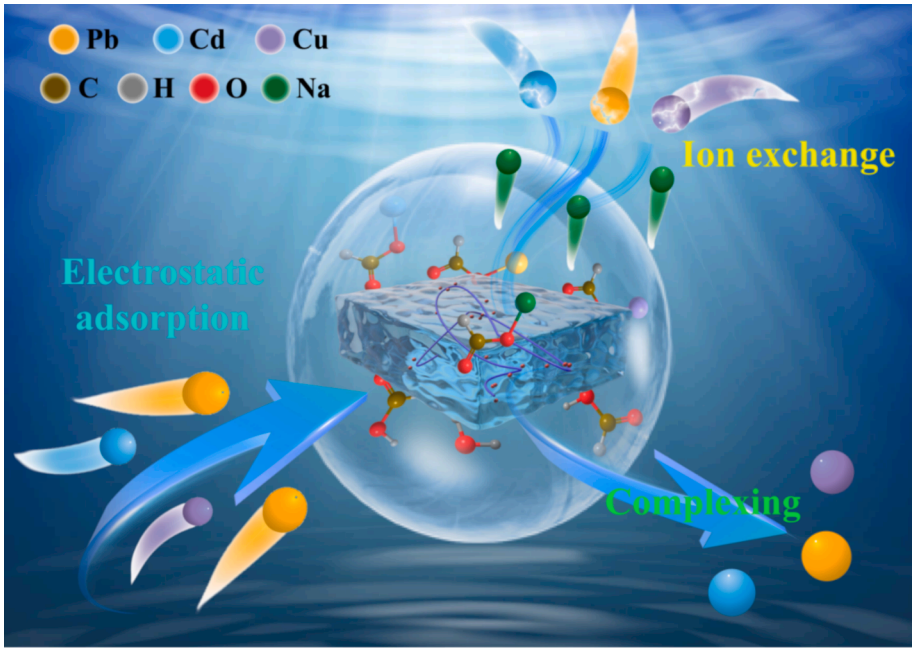

Fig. 8. Potential mechanism diagram of adsorption of three heavy metals by RMAAC.

sodium decreased from 47 % prior to the adsorption of these three heavy metals to 16 %, 2 %, and 4 %, respectively. Furthermore, the content of Pb, Cd, and Cu elements after adsorption amounts to 35 %, 77 %, and 47 %, respectively. This phenomenon suggests that ion exchange serves as the primary mechanism driving the adsorption process (Wu et al., 2021).

3.3.4. *XPS characterization*

In order to gain further insights into the adsorption mechanism of heavy metals by RMAAC, XPS analysis was conducted on the RMAAC sample. The obtained results are presented in Fig. 7. From the overall XPS spectrum (Fig. 7a), it is evident that the characteristic peaks corresponding to sodium elements disappear after the adsorption of heavy metals. Conversely, the characteristic peaks of Pb4f, Cd3d, and Cu2p emerge following the adsorption process (Fig. 7b–d). These findings indicate that RMAAC effectively adsorbs these three heavy metals, with the primary ion-exchange process involving sodium ions. Remarkably, these results are consistent with the findings obtained from the SEM-EDS analysis.

From the deconvolution results of Cu2p (Fig. 7d), it is evident that Cu exists in both Cu(I) and Cu(II) forms, with the corresponding binding energies of the two groups of characteristic peaks being 952.68, 932.98, 954.58, and 934.88 eV, respectively. Additionally, a set of satellite characteristic peaks has combined energies of 944.18 eV and 939.88 eV, which correspond to the satellite peaks of Cu(II) and Cu(I), respectively (Ding et al., 2024). The C1s spectrum of RMAAC exhibits three peaks (Fig. 7e), representing C–C, C-O, and C = C. The corresponding central binding energies are 284.67, 286.46, and 287.97 eV, respectively. The O1s spectrum shows four characteristic peaks (Fig. 7f), which correspond to oxygen-containing functional groups O = C, O–H, O-C, and sodium elements (Cai et al., 2023). The central binding energies of these peaks are 530.96, 531.76, 533.15, and 535.64 eV, respectively.

Upon adsorption of these three heavy metals by RMAAC, the peak area and location of the C–C characteristic peaks of C1s do not change significantly (Fig. 7e). The position of the C-O characteristic peaks remains relatively stable, but the peak area increases. This indicates that C-O functional groups can react with heavy metal ions during the adsorption process, forming stable metal complexes by sharing electron pairs with oxygen atoms (Xie et al., 2023). This observation is consistent with the changes observed in the C-O characteristic peaks of O1s. The area of the characteristic peaks of C = O does not change significantly, but the peak positions shift to 288.43, 288.61, and 288.56 eV, respectively, with a displacement change of more than 0.5 eV. This shift can be attributed to the formation of complexes between heavy metal ions and carboxylic acid groups, leading to a decreased density of electron clouds around carbon atoms and a shift towards higher binding energy (Xia et al., 2020). The characteristic peaks of sodium element in the O1s spectrum disappear after adsorption of these three heavy metals by RMAAC (Fig. 7f), confirming the consumption of sodium element during the ion exchange process. The area of the O–H characteristic peak decreases significantly, and the central peak shifts to 532.03, 532.11, and 532.43 eV, respectively. The area of the O = C characteristic peaks shows no significant change, and the central peaks shift to 531.17, 531.53, and 531.64 eV, respectively. The peak position of the O-C characteristic peak remains relatively unchanged, but the peak area increases. By comparing the characteristic peaks of C1s and O1s before and after adsorption, it is observed that certain peaks shift towards higher binding energy, with differences in peak positions before and after adsorption exceeding 0.5 eV. Therefore, it can be concluded that oxygen-containing functional groups in RMAAC form complexes with heavy metal ions through chelation coordination (Ma et al., 2018a).

3.3.5. *Adsorption mechanism analysis*

XRD analysis revealed that the adsorption of heavy metals by RMAAC did not result in the formation of distinct crystals. Instead, broad diffraction peaks were observed after adsorption. FTIR analysis unveiled that the hydroxyl (O–H) and carboxyl (O-C = O) groups present in RMAAC played a pivotal role. SEM-EDS characterization demonstrated noticeable alterations in the morphology of RMAAC before and after adsorption, suggesting the occurrence of an evident ion exchange process. Based on these analyses, combined with the results of XPS, a potential adsorption mechanism was proposed, as depicted in Fig. 8. Initially, RMAAC absorbed these three heavy metals by electrostatic attraction. Subsequently, RMAAC engages in an ion-exchange process to facilitate the adsorption of heavy metal ions, utilizing the presence of Na element (Figs. 6 and 7). Furthermore, the oxygen-containing functional groups present in RMAAC form complexes with heavy metals through chelating coordination (Figs. 5 and 7), thereby facilitating the adsorption of heavy metal ions.

4. Conclusion

Red mud/polyacrylic acid/sodium carboxymethyl cellulose hydrogel (RMAAC) was successfully synthesized through free radical polymerization. The response surface method was utilized to optimize the optimal combination ratio of each component in RMAAC, resulting in the following ratios: MBA 0.15 %, KPS 0.2 %, SCMC 1.5 %, along with the addition of 0.5 % RM to enhance the adsorption performance of the hydrogel. The adsorption performance of RMAAC for Pb(II), Cd(II), and Cu(II) was found to be relatively high within a pH range of 3 to 6. The adsorption process followed the pseudo-second-order kinetic and Langmuir model. The primary mode of adsorption was single-molecular layer chemisorption, while the intra-particle diffusion process was dominated by liquid film diffusion. At 25°C, the theoretical maximum adsorption capacities were determined to be 730.16, 292.71, and 215.37 mg/g for Pb(II), Cd(II), and Cu(II) respectively. In the multi-heavy metal system, RMAAC exhibited a higher adsorption capacity for Pb(II) compared to Cu(II) and Cd(II). Characterization techniques including XRD, FTIR, SEM-EDS, and XPS were employed to investigate the adsorption mechanism of these three heavy metals by RMAAC. Ion exchange and coordination chelation were identified as the main adsorption mechanisms. Overall, the synthesized RMAAC hydrogel demonstrated promising adsorption capabilities for removing heavy metal ions from water sources. These findings contribute to addressing the urgent environmental concerns related to heavy metal pollution and red mud disposal, providing a potential solution for the effective utilization of red mud waste.

CRediT authorship contribution statement

Dong Zhao: Writing – original draft, Validation, Software, Formal analysis, Data curation. **Hua Deng:** Writing – review & editing, Supervision, Resources, Project administration, Funding acquisition. **Wei Wang:** Writing – review & editing, Methodology, Investigation, Formal analysis. **Lening Hu:** Validation, Supervision. **Shunyun Ye:** Validation, Methodology. **Jiahui Fu:** Validation, Formal analysis. **Shuyun Zhang:** Validation, Investigation.

Declaration of Competing Interest

The authors declare that they have no known competing financial interests or personal relationships that could have appeared to influence the work reported in this paper.

Acknowledgements

This work was funded by the Key R&D Program of Guangxi, China (Grant No. AB22035038). We owe thank the Key Laboratory of Ecology of Rare and Endangered Species and Environmental Protection (Guangxi Normal University), Ministry of Education, for their help with experimental test. Finally, the authors would like to thank the Key Laboratory of Medicinal Resource Chemistry and Pharmaceutical Molecular Engineering (Guangxi Normal University) for providing testing instruments for FTIR, XPS and XRD.

Appendix A. Supplementary data

Supplementary data to this article can be found online at https://doi.org/10.1016/j.arabjc.2024.106067.

References

Abdel-Magied, A.F., Abdelhamid, H.N., Ashour, R.M., Fu, L., Dowaidar, M., Xia, W., Forsberg, K., 2022. Magnetic metal-organic frameworks for efficient removal of cadmium(II), and lead(II) from aqueous solution. J. Environ. Chem. Eng. 10, 107467. https://doi.org/10.1016/j.jece.2022.107467.

Agrawal, S., Dhawan, N., 2021. Evaluation of red mud as a polymetallic source – A review. Miner. Eng. 171, 107084. https://doi.org/10.1016/j.mineng.2021.107084.

Ahmed, W., Mehmood, S., Mahmood, M., Ali, S., Shakoor, A., Núñez-Delgado, A., Asghar, R.M.A., Zhao, H., Liu, W., Li, W., 2023. Adsorption of Pb(II) from wastewater using a red mud modified rice-straw biochar: Influencing factors and reusability. Environ. Pollut. 326, 121405. https://doi.org/10.1016/j.envpol.2023.121405.

Akl, M.A., Hashem, M.A., Ismail, M.A., Abdelgalil, D.A., 2022. Novel diaminoguanidine functionalized cellulose: synthesis, characterization, adsorption characteristics and application for ICP-AES determination of copper(II), mercury(II), lead(II) and cadmium(II) from aqueous solutions. BMC Chem. 16, 65. https://doi.org/10.1186/s13065-022-00857-3.

Arroyo, F., Luna-Galiano, Y., Leiva, C., Vilches, L.F., Fernández-Pereira, C., 2020. Environmental risks and mechanical evaluation of recycling red mud in bricks. Environ. Res. 186, 109537. https://doi.org/10.1016/j.envres.2020.109537.

Azeem, M.K., Rizwan, M., Islam, A., Rasool, A., Khan, S.M., Khan, R.U., Rasheed, T., Bilal, M., Iqbal, H.M.N., 2022. In-house fabrication of macro-porous biopolymeric hydrogel and its deployment for adsorptive remediation of lead and cadmium from water matrices. Environ. Res. 214, 113790. https://doi.org/10.1016/j.envres.2022.113790.

Bai, X., Lin, J., Zhang, Z., Zhan, Y., 2022. Immobilization of lead, copper, cadmium, nickel, and zinc in sediment by red mud: adsorption characteristics, mechanism, and effect of dosage on immobilization efficiency. Environ Sci Pollut Res 29, 51793–51814. https://doi.org/10.1007/s11356-022-19506-2.

Bai, Y., Pang, Y., Wu, Z., Li, X., Jing, J., Wang, H., Zhou, Z., 2023. Adsorption of Lead from Water Using MnO_2-Modified Red Mud: Performance, Mechanism, and Environmental Risk. Water 15, 4314. https://doi.org/10.3390/w15244314.

Bao, Q., Nie, W., Liu, C., Zhang, H., Wang, H., Jin, H., Yan, J., Liu, Q., 2020. The preparation of a novel hydrogel based on crosslinked polymers for suppressing coal dusts. J. Clean. Prod. 249, 119343. https://doi.org/10.1016/j.jclepro.2019.119343.

Bashir, A., Malik, L.A., Ahad, S., Manzoor, T., Bhat, M.A., Dar, G.N., Pandith, A.H., 2019. Removal of heavy metal ions from aqueous system by ion-exchange and biosorption methods. Environ Chem Lett 17, 729–754. https://doi.org/10.1007/s10311-018-00828-y.

Bilal, M., Ihsanullah, I., Younas, M., Ul Hassan Shah, M., 2021. Recent advances in applications of low-cost adsorbents for the removal of heavy metals from water: A critical review. Separation and Purification Technology 278, 119510. 10.1016/j.seppur.2021.119510.

Cai, B., Li, M., Zhou, J., Tan, L., Li, D., Ao, Z., 2023. Effect of oxygen-containing functional groups at SWCNT on the formation of sodium and lithium dendrites. Surf. Interfaces 40, 103074. https://doi.org/10.1016/j.surfin.2023.103074.

Chakraborty, R., Asthana, A., Singh, A.K., Jain, B., Susan, A.B.H., 2022. Adsorption of heavy metal ions by various low-cost adsorbents: a review. Int. J. Environ. Anal. Chem. 102, 342–379. https://doi.org/10.1080/03067319.2020.1722811.

Cortés, J.-C., Navarro-Quiles, A., Santonja, F.-J., Sferle, S.-M., 2023. Statistical analysis of randomized pseudo-first/second order kinetic models. Application to study the adsorption on cadmium ions onto tree fern. Chemom. Intel. Lab. Syst. 240, 104910. https://doi.org/10.1016/j.chemolab.2023.104910.

Darban, Z., Shahabuddin, S., Gaur, R., Ahmad, I., Sridewi, N., 2022. Hydrogel-Based Adsorbent Material for the Effective Removal of Heavy Metals from Wastewater: A Comprehensive Review. Gels 8, 263. https://doi.org/10.3390/gels8050263.

Ding, W., Sun, H., Li, X., Li, Y., Jia, H., Luo, Y., She, D., Geng, Z., 2024. Environmental applications of lignin-based hydrogels for Cu remediation in water and soil: adsorption mechanisms and passivation effects. Environ. Res. 250, 118442. https://doi.org/10.1016/j.envres.2024.118442.

El Sayed, M.M., 2023. Production of Polymer Hydrogel Composites and Their Applications. J Polym Environ 31, 2855–2879. https://doi.org/10.1007/s10924-023-02796-z.

Elwakeel, K.Z., Ahmed, M.M., Akhdhar, A., Alghamdi, H.M., Sulaiman, M.G.M., Hamza, M.F., Khan, Z.A., 2023. Effect of the magnetic core in alginate/gum composite on adsorption of divalent copper, cadmium, and lead ions in the aqueous system. Int. J. Biol. Macromol. 253, 126884. https://doi.org/10.1016/j.ijbiomac.2023.126884.

Enoch, K., Somasundaram, A.A., 2023. Rheological insights on Carboxymethyl cellulose hydrogels. Int. J. Biol. Macromol. 253, 127481. https://doi.org/10.1016/j.ijbiomac.2023.127481.

Feng, Z., Feng, C., Chen, N., Wang, S., 2023. Self-polymerization magnetic hydrogel for Cu and Pb adsorption from aqueous solutions: Theoretical insight and implication. Colloid Surf. A-Physicochem. Eng. Asp. 677, 132298. https://doi.org/10.1016/j.colsurfa.2023.132298.

Fu, Z.-J., Jiang, S.-K., Chao, X.-Y., Zhang, C.-X., Shi, Q., Wang, Z.-Y., Liu, M.-L., Sun, S.-P., 2022. Removing miscellaneous heavy metals by all-in-one ion exchange-nanofiltration membrane. Water Res. 222, 118888. https://doi.org/10.1016/j.watres.2022.118888.

Gururajan, K., Belur, P.D., 2018. Screening and selection of indigenous metal tolerant fungal isolates for heavy metal removal. Environ. Technol. Innov. 9, 91–99. https://doi.org/10.1016/j.eti.2017.11.001.

Hong, M., Yu, L., Wang, Y., Zhang, J., Chen, Z., Dong, L., Zan, Q., Li, R., 2019. Heavy metal adsorption with zeolites: The role of hierarchical pore architecture. Chem. Eng. J. 359, 363–372. https://doi.org/10.1016/j.cej.2018.11.087.

Jiang, J., Shi, Y., Ma, N.L., Ye, H., Verma, M., Ng, H.S., Ge, S., 2024. Utilizing adsorption of wood and its derivatives as an emerging strategy for the treatment of heavy metal-contaminated wastewater. Environ. Pollut. 340, 122830. https://doi.org/10.1016/j.envpol.2023.122830.

Jiao, R., Lou, T., Zhang, H., Wang, X., 2022. Preparation of starch-acrylic acid-carboxymethyl cellulose copolymer and its flocculation performance towards

methylene blue. Biochem. Eng. J. 187, 108635. https://doi.org/10.1016/j.bej.2022.108635.
Jing, K., Liu, X., Liu, T., Wang, Z., Liu, H., 2023. Facile and green construction of carboxymethyl cellulose-based aerogel to efficiently and selectively adsorb cationic dyes. J. Water Process Eng. 56, 104386. https://doi.org/10.1016/j.jwpe.2023.104386.
Ke, Z., Chen, Z., Xiao, Y., Tang, F., Zhang, S., 2024. Adsorption of PO43−, Cd(II), Pb(II), Cu(II), As(III), and As(V) using the La-based and modified La-based metal–organic framework materials. J. Mol. Struct. 1307, 138005. https://doi.org/10.1016/j.molstruc.2024.138005.
Kuang, J., Cai, T., Dai, J., Yao, L., Liu, F., Liu, Y., Shu, J., Fan, J., Peng, H., 2023. High strength chitin/chitosan-based aerogel with 3D hierarchically macro-meso-microporous structure for high-efficiency adsorption of Cu(II) ions and Congo red. Int. J. Biol. Macromol. 230, 123238. https://doi.org/10.1016/j.ijbiomac.2023.123238.
Li, T., Liu, X., Li, L., Wang, Y., Ma, P., Chen, M., Dong, W., 2019. Polydopamine-functionalized graphene oxide compounded with polyvinyl alcohol/chitosan hydrogels on the recyclable adsorption of cu(II), Pb(II) and cd(II) from aqueous solution. J Polym Res 26, 281. https://doi.org/10.1007/s10965-019-1971-6.
Li, S.-S., Song, Y.-L., Yang, H.-R., An, Q.-D., Xiao, Z.-Y., Zhai, S.-R., 2020. Carboxymethyl cellulose-based cryogels for efficient heavy metal capture: Aluminum-mediated assembly process and sorption mechanism. Int. J. Biol. Macromol. 164, 3275–3286. https://doi.org/10.1016/j.ijbiomac.2020.08.186.
Li, S., Zheng, Z., Xia, S., Hu, J., Chen, L., Huang, L., Song, Q., Shen, X., Zhang, W., 2023. Fabrication of bamboo cellulose-based nanofiltration membrane for water purification by cross-linking sodium alginate and carboxymethyl cellulose and its dynamics simulation. Chem. Eng. J. 473, 145403. https://doi.org/10.1016/j.cej.2023.145403.
Liang, J., Li, X., Yu, Z., Zeng, G., Luo, Y., Jiang, L., Yang, Z., Qian, Y., Wu, H., 2017. Amorphous MnO $_2$ Modified Biochar Derived from Aerobically Composted Swine Manure for Adsorption of Pb(II) and Cd(II). ACS Sustainable Chem. Eng. 5, 5049–5058. https://doi.org/10.1021/acssuschemeng.7b00434.
Liang, C., Meng, S., Wang, Y., Xie, X., Zhang, Z., Cheng, D., 2023. Preparation and activity of sodium carboxymethyl cellulose (CMC-Na) and *Metarhizium rileyi* ZHKUMR1 composite membrane. Int. J. Biol. Macromol. 253, 126858. https://doi.org/10.1016/j.ijbiomac.2023.126858.
Lin, Z., Yang, Y., Liang, Z., Zeng, L., Zhang, A., 2021. Preparation of Chitosan/Calcium Alginate/Bentonite Composite Hydrogel and Its Heavy Metal Ions Adsorption Properties. Polymers 13, 1891. https://doi.org/10.3390/polym13111891.
Liu, L., 2023. A comprehensive model of adsorption of resorcinol in rotating packed bed: Theoretical, isotherm, kinetics and thermodynamics. J. Environ. Chem. Eng. 11, 111041. https://doi.org/10.1016/j.jece.2023.111041.
Liu, Q., Li, Z., Ma, Q., Li, X., Li, G., Zeng, F., Shao, Z., 2022. Preparation and properties of ZnMoO4 anode materials with polymer network gel method. J. Indian Chem. Soc. 99, 100491. https://doi.org/10.1016/j.jics.2022.100491.
Liu, Y., Naidu, R., 2014. Hidden values in bauxite residue (red mud): Recovery of metals. Waste Manag. 34, 2662–2673. https://doi.org/10.1016/j.wasman.2014.09.003.
Liu, M., Wang, Y., Wu, Y., Liu, C., Liu, X., 2023. Preparation of Graphene Oxide Hydrogels and Their Adsorption Applications toward Various Heavy Metal Ions in Aqueous Media. Appl. Sci. 13, 11948. https://doi.org/10.3390/app132111948.
Liu, J., Xie, Y., Li, C., Fang, G., Chen, Q., Ao, X., 2020. Novel red mud/polyacrylic composites synthesized from red mud and its performance on cadmium removal from aqueous solution. J of Chemical Tech & Biotech 95, 213–222. https://doi.org/10.1002/jctb.6223.
Lunardi, V.B., Santoso, S.P., Angkawijaya, A.E., Cheng, K.-C., Tran-Nguyen, P.L., Go, A. W., Nakamura, Y., Lin, S.-P., Hsu, H.-Y., Yuliana, M., Soetaredjo, F.E., Ismadji, S., 2024. Synthesis of cellulose hydrogel by utilizing agricultural waste and zeolite for adsorption of copper metal ions. Ind. Crop. Prod. 210, 118179. https://doi.org/10.1016/j.indcrop.2024.118179.
Lyu, F., Niu, S., Wang, L., Liu, R., Sun, W., He, D., 2021. Efficient removal of Pb(II) ions from aqueous solution by modified red mud. J. Hazard. Mater. 406, 124678. https://doi.org/10.1016/j.jhazmat.2020.124678.
Ma, Y., Deng, Z., Li, Z., Lin, Q., Wu, Y., Dou, W., 2021. Adsorption characteristics and mechanism for K2Ti4O9 whiskers removal of Pb(II), Cd(II), and Cu(II) cations in wastewater. J. Environ. Chem. Eng. 9, 106236. https://doi.org/10.1016/j.jece.2021.106236.
Ma, J., Luo, J., Liu, Y., Wei, Y., Cai, T., Yu, X., Liu, H., Liu, C., Crittenden, J.C., 2018a. J. Mater. Chem. A 6, 20110–20120. https://doi.org/10.1039/C8TA07250G.
Ma, J., Zhang, Y., Tang, Y., Wei, Y., Liu, Y., Liu, C., 2018b. Efficient removal of heavy metals from melting effluent using multifunctional hydrogel adsorbents. Water Sci. Technol. 78, 982–990. https://doi.org/10.2166/wst.2018.380.
Malik, L.A., Bashir, A., Qureashi, A., Pandith, A.H., 2019. Detection and removal of heavy metal ions: a review. Environ Chem Lett 17, 1495–1521. https://doi.org/10.1007/s10311-019-00891-z.
Milosavljevic, N.B., Ristic, M.D., Peric-Grujic, A.A., Filipovic, J.M., Strbac, S.B., Rakocevic, Z.L., Krusic, M.T.K., 2010. Hydrogel based on chitosan, itaconic acid and methacrylic acid as adsorbent of Cd²⁺ ions from aqueous solution. Chem. Eng. J. 165, 554–562. https://doi.org/10.1016/j.cej.2010.09.072.
Nassef, H.M., Al-Hazmi, G.A.A.M., Alayyafi, A.A., El-Desouky, M.G., El-Bindary, A.A., 2024. Synthesis and characterization of new composite sponge combining of metal-organic framework and chitosan for the elimination of Pb(II), Cu(II) and Cd(II) ions from aqueous solutions: Batch adsorption and optimization using Box-Behnken design. J. Mol. Liq. 394, 123741. https://doi.org/10.1016/j.molliq.2023.123741.
Niu, A., Lin, C., 2024. Trends in research on characterization, treatment and valorization of hazardous red mud: A systematic review. J. Environ. Manage. 351, 119660. https://doi.org/10.1016/j.jenvman.2023.119660.
Noor, A.E., Fatima, R., Aslam, S., Hussain, A., Nisa, Z. un, Khan, M., Mohammed, A.A.A., Sillanpaa, M., 2024. Health risks assessment and source admeasurement of potentially dangerous heavy metals (Cu, Fe, and Ni) in rapidly growing urban settlement. Environmental Research 242, 117736. 10.1016/j.envres.2023.117736.
Omrani, N., Nezamzadeh-Ejhieh, A., 2020. Focus on scavengers' effects and GC-MASS analysis of photodegradation intermediates of sulfasalazine by Cu2O/CdS nanocomposite. Sep. Purif. Technol. 235, 116228. https://doi.org/10.1016/j.seppur.2019.116228.
Pan, X., Wu, H., Lv, Z., Yu, H., Tu, G., 2023. Recovery of valuable metals from red mud: A comprehensive review. Sci. Total Environ. 904, 166686. https://doi.org/10.1016/j.scitotenv.2023.166686.
Qi, J., Zhu, H., Yang, T., Wang, X., Wang, Z., Lei, X., Li, B., Qian, W., 2024. Biomass-derived carbon/iron composite (FexOy-BC (RM)) with excellent Cd(II) adsorption from wastewater – Red mud resource utilization. Arab. J. Chem. 17, 105411. https://doi.org/10.1016/j.arabjc.2023.105411.
Rajendran, S., Priya, A.K., Senthil Kumar, P., Hoang, T.K.A., Sekar, K., Chong, K.Y., Khoo, K.S., Ng, H.S., Show, P.L., 2022. A critical and recent developments on adsorption technique for removal of heavy metals from wastewater-A review. Chemosphere 303, 135146. https://doi.org/10.1016/j.chemosphere.2022.135146.
Ramírez, A., Gómez, L., Müller, A.J., Rojas De Gáscue, B., 2022. Characterization and Modification of Red Mud and Ferrosilicomanganese Fines and Their Application in the Synthesis of Hybrid Hydrogels. Polymers 14, 4330. https://doi.org/10.3390/polym14204330.
Sandu, T., Sarbu, A., Zavoianu, R., Spatarelu, C.P., Florea, M., Bradu, C., Mara, E.L., Dragut, D.V., Alexandrescu, E., Zaharia, A., Radu, A.L., 2017. New ways to use the red mud waste as raw material for inorganic- organic hybrid hydrogels. Int. J. Miner. Process. 169, 111–118. https://doi.org/10.1016/j.minpro.2017.11.005.
Singh, V., Singh, N., Rai, S.N., Kumar, A., Singh, A.K., Singh, M.P., Sahoo, A., Shekhar, S., Vamanu, E., Mishra, V., 2023. Heavy Metal Contamination in the Aquatic Ecosystem: Toxicity and Its Remediation Using Eco-Friendly Approaches. Toxics 11, 147. https://doi.org/10.3390/toxics11020147.
Sun, Z., Yin, Y., An, Y., Deng, C., Wei, Z., Jiang, Z., Duan, X., Xu, X., Chen, J., 2022. A novel modified carboxymethyl cellulose hydrogel adsorbent for efficient removal of poisonous metals from wastewater: Performance and mechanism. J. Environ. Chem. Eng. 10, 108179. https://doi.org/10.1016/j.jece.2022.108179.
Tang, S., Yang, J., Lin, L., Peng, K., Chen, Y., Jin, S., Yao, W., 2020. Construction of physically crosslinked chitosan/sodium alginate/calcium ion double-network hydrogel and its application to heavy metal ions removal. Chem. Eng. J. 393, 124728. https://doi.org/10.1016/j.cej.2020.124728.
Tsamo, C., Djomou Djonga, P.N., Dangwang Dikdim, J.M., Kamga, R., 2018. Kinetic and Equilibrium Studies of Cr(VI), Cu(II) and Pb(II) Removal from Aqueous Solution Using Red Mud, a Low-Cost Adsorbent. Arab J Sci Eng 43, 2353–2368. https://doi.org/10.1007/s13369-017-2787-5.
Vardhan, K.H., Kumar, P.S., Panda, R.C., 2019. A review on heavy metal pollution, toxicity and remedial measures: Current trends and future perspectives. J. Mol. Liq. 290, 111197. https://doi.org/10.1016/j.molliq.2019.111197.
Wang, S., Jin, H., Deng, Y., Xiao, Y., 2021. Comprehensive utilization status of red mud in China: A critical review. J. Clean. Prod. 289, 125136. https://doi.org/10.1016/j.jclepro.2020.125136.
Wang, L., Sun, N., Tang, H., Sun, W., 2019. A Review on Comprehensive Utilization of Red Mud and Prospect Analysis. Minerals 9, 362. https://doi.org/10.3390/min9060362.
Wen, Y., Xue, C., Ji, D., Hou, Y., Li, K., Li, Y., 2023. Eco-friendly Enteromorpha polysaccharides-based hydrogels for heavy metal adsorption: From waste to efficient materials. Colloid Surf. A-Physicochem. Eng. Asp. 656, 130531. https://doi.org/10.1016/j.colsurfa.2022.130531.
Wu, Y., Li, C., 2023. A double-layer smart film based on gellan gum/modified anthocyanin and sodium carboxymethyl cellulose/starch/Nisin for application in chicken breast. Int. J. Biol. Macromol. 232, 123464. https://doi.org/10.1016/j.ijbiomac.2023.123464.
Wu, J., Wang, T., Wang, J., Zhang, Y., Pan, W.-P., 2021. A novel modified method for the efficient removal of Pb and Cd from wastewater by biochar: Enhanced the ion exchange and precipitation capacity. Sci. Total Environ. 754, 142150. https://doi.org/10.1016/j.scitotenv.2020.142150.
Xi, Y., Xie, T., Liu, Y., Wu, Y., Liu, H., Su, Z., Huang, Y., Yuan, X., Zhang, C., Li, X., 2022. Carboxymethyl cellulose stabilized ferrous sulfide@extracellular polymeric substance for Cr(VI) removal: Characterization, performance, and mechanism. J. Hazard. Mater. 425, 127837. https://doi.org/10.1016/j.jhazmat.2021.127837.
Xia, L., Lu, Y., Meng, H., Li, C., 2020. Preparation of C-MOx nanocomposite for efficient adsorption of heavy metal ions via mechanochemical reaction of CaC2 and transitional metal oxides. J. Hazard. Mater. 393, 122487. https://doi.org/10.1016/j.jhazmat.2020.122487.
Xie, Z., Diao, S., Xu, R., Wei, G., Wen, J., Hu, G., Tang, T., Jiang, L., Li, X., Li, M., Huang, H., 2023. Construction of carboxylated-GO and MOFs composites for efficient removal of heavy metal ions. Appl. Surf. Sci. 636, 157827. https://doi.org/10.1016/j.apsusc.2023.157827.
Xie, W.-M., Zhou, F.-P., Bi, X.-L., Chen, D.-D., Li, J., Sun, S.-Y., Liu, J.-Y., Chen, X.-Q., 2018. Accelerated crystallization of magnetic 4A-zeolite synthesized from red mud for application in removal of mixed heavy metal ions. J. Hazard. Mater. 358, 441–449. https://doi.org/10.1016/j.jhazmat.2018.07.007.
Xu, R., Wei, G., Xie, Z., Diao, S., Wen, J., Tang, T., Jiang, L., Li, M., Hu, G., 2024. V2C MXene–modified g-C3N4 for enhanced visible-light photocatalytic activity. J. Alloy. Compd. 970, 172656. https://doi.org/10.1016/j.jallcom.2023.172656.
Yin, L., Deng, Q., Ke, Z., Yu, Q., Xiao, Y., Zhang, S., 2023. Synthesis, modification, and adsorption properties of Yb-MOF: Kinetic and thermodynamic studies. Appl. Organomet. Chem. 37, e6955.

Zhang, Q., Cao, X., Sun, S., Yang, W., Fang, L., Ma, R., Lin, C., Li, H., 2022. Lead zinc slag-based geopolymer: Demonstration of heavy metal solidification mechanism from the new perspectives of electronegativity and ion potential. Environ. Pollut. 293, 118509. https://doi.org/10.1016/j.envpol.2021.118509.

Zhang, Z., Li, J., Meng, N., Song, S., Zhu, Q., Li, D., Gong, L., Ding, Y., Zhang, R., Shi, X., 2024. Simultaneously-efficient electro-sorption of Pb(II), Cu(II) and Cd(II) by Cu2+ modified superactive carbons. Sep. Purif. Technol. 338, 126604. https://doi.org/10.1016/j.seppur.2024.126604.

Zhang, L., Tang, S., He, F., Liu, Y., Mao, W., Guan, Y., 2019. Highly efficient and selective capture of heavy metals by poly(acrylic acid) grafted chitosan and biochar composite for wastewater treatment. Chem. Eng. J. 378, 122215. https://doi.org/10.1016/j.cej.2019.122215.

Zhang, Y., Zhao, M., Cheng, Q., Wang, C., Li, H., Han, X., Fan, Z., Su, G., Pan, D., Li, Z., 2021. Research progress of adsorption and removal of heavy metals by chitosan and its derivatives: A review. Chemosphere 279, 130927. https://doi.org/10.1016/j.chemosphere.2021.130927.

Zhao, Z., Huang, Y., Wu, Y., Li, S., Yin, H., Wang, J., 2021. α-ketoglutaric acid modified chitosan/polyacrylamide semi-interpenetrating polymer network hydrogel for removal of heavy metal ions. Colloids Surf A Physicochem Eng Asp 628, 127262. https://doi.org/10.1016/j.colsurfa.2021.127262.

Zhao, Z., Wang, B., Feng, Q., Chen, M., Zhang, X., Zhao, R., 2023. Recovery of nitrogen and phosphorus in wastewater by red mud-modified biochar and its potential application. Sci. Total Environ. 860, 160289. https://doi.org/10.1016/j.scitotenv.2022.160289.

Zhou, Z., Sun, Y., Wang, Y., Yu, F., Ma, J., 2022. Adsorption behavior of Cu(II) and Cr(VI) on aged microplastics in antibiotics-heavy metals coexisting system. Chemosphere 291, 132794. https://doi.org/10.1016/j.chemosphere.2021.132794.

Zou, Y., 2024. Cu²⁺, Cd²⁺, and Pb²⁺ ions adsorption from wastewater using polysaccharide hydrogels made of oxidized carboxymethyl cellulose and chitosan grafted with catechol groups. Iran. Polym. J. 33, 57–66. https://doi.org/10.1007/s13726-023-01234-0.